ORIGINAL RESEARCH

Fe₃O₄@Polydopamine-Labeled MSCs Targeting the Spinal Cord to Treat Neuropathic Pain Under the Guidance of a Magnetic Field

Meichen Liu[1]
Weijia Yu[2]
Fuqiang Zhang[2]
Te Liu[2]
Kai Li[1]
Meng Lin [ID][3]
Ying Wang[2]
Guoqing Zhao[1]
Jinlan Jiang[2]

[1]Department of Anesthesiology, China-Japan Union Hospital of Jilin University, Changchun, Jilin, People's Republic of China; [2]Department of Scientific Research Center, China-Japan Union Hospital of Jilin University, Changchun, Jilin, People's Republic of China; [3]Department of Breast Surgery, The First Hospital of Jilin University, Changchun, Jilin, People's Republic of China

Purpose: Neuropathic pain causes great distress among patients; however, its response to traditional analgesia techniques remains sub-optimal. There has been progress in stem cell research for neuropathic pain treatment; however, effective homing remains problematic. This study aimed to establish Fe₃O₄@polydopamine(PDA)-labeled mesenchymal stem cells (MSCs); moreover, we aimed to guide MSCs using a magnetic field to the spinal cord segments showing pain-related responses to allow MSC homing and gathering, in advance, in order to fully employ their repair function.

Materials and Methods: Fe₃O₄@PDA-labeled MSCs were characterized using transmission electron microscopy. We analyzed the characteristics of MSCs, as well as the nanoparticle effects on MSC activity, differentiation, and proliferation, using the CCK-8 method, flow cytometry, and staining. Using rats, we performed behavioral tests of mechanical and thermal pain hypersensitivity. Serum inflammatory markers were detected using ELISA. Finally, changes in proteins associated with spinal cord pain were detected through quantitative reverse transcription PCR, histology, and immunohistochemistry.

Results: Fe₃O₄@PDA did not affect the characteristics and viability of MSCs. The magnetic field guidance improved the therapeutic effect of Fe₃O₄@PDA-labeled MSCs as indicated by the paw withdrawal threshold. Fe₃O₄@PDA-labeled MSCs decreased spinal nerve demyelination and c-Fos expression (a pain molecule); moreover, they inhibited microglia and astrocyte activation.

Conclusion: Fe₃O₄@PDA-labeled MSCs showed better homing to the spinal cord under magnetic field guidance. Moreover, they inhibited microglial and astrocyte activation, as well as played an early and continuous role in neuropathic pain treatment.

Keywords: Fe₃O₄@PDA, MSCs, neuropathic pain, microglia, astrocytes

Introduction

Neuropathic pain is caused by lesions or diseases of the somatosensory nervous system. It is often expressed in the somatic form (projective pain) in the innervated structure of the neuropathic area. Neuropathic pain may be spontaneous or induced by sensory stimulation (hyperalgesia and allodynia).[1] Clinically, various diseases can cause neuropathic pain, including painful peripheral neuropathy, post-herpetic neuralgia, traumatic nerve injury, spinal cord injury, diabetic neuralgia, lumbar or cervical radiculopathy, multiple sclerosis, and others.[2] The estimated prevalence of neuropathic pain in the general population ranges from 6.9% to 10%.[3] Neuropathic pain affects numerous aspects of daily life and is associated with poor overall

Correspondence: Guoqing Zhao;
Jinlan Jiang
No. 126, Xiantai Street, Changchun City, Jilin Province, People's Republic of China
Email guoqing@jlu.edu.cn;
jiangjinlan@jlu.edu.cn

3275

health, poor quality of life, poor sleep, high anxiety, and depression, which are more severe than those observed in nociceptive pain.[4,5] However, although drug therapy is the main tool for effective pain control, neuropathic pain shows a suboptimal response to traditional analgesic techniques.[6–8]

In the last two decades, stem cell transplantation has been investigated as a possible treatment for neuropathic pain.[9–12] Mesenchymal stem cells (MSCs) can easily grow in vitro and have notable characteristics of immunomodulatory properties, non-teratogenicity, and multi-potential with high genetic stability. Additionally, they can improve synaptic transmission and promote neural networks.[13–16] Initially, it was thought that stem cells could replace damaged nerve cells and deliver nutritional factors to the diseased site based on the stem cell potency. However, intensive research has revealed that the utility of stem cells in neuropathic pain is not dependent on their regenerative effects. Rather, it is mainly associated with the two-way interaction between stem and resident cells in the damaged microenvironment.[17] Given the reported transplantation safety and efficacy under certain conditions, there has been rapid development in the use of MSCs as therapeutic agents. Mazzini et al[18] reported that intravenous MSC administration to patients with amyotrophic lateral sclerosis was safe for up to 9 years; moreover, there were no adverse events in a clinical trial of human stem cells that included 53 participants.[19]

Although MSCs can undergo high-level in vitro expansion and have wide clinical applications, to facilitate successful implantation, there remains a huge challenge in effectively transporting MSCs to the target site. MSCs have shown low efficiency in targeting damaged or inflamed tissues.[20] Currently, preclinical experiments on stem cell treatment of neuropathic pain have employed intrathecal or tail vein injections to automatically target spinal cord cells or the corresponding injured area. After tail vein injection, most stem cells are trapped in the lungs.[21] Waiting for the cells to detach from the lungs and return to the damaged tissues inevitably lengthens the time taken to achieve therapeutic effects. As an invasive drug administration method, intrathecal injection not only has numerous clinical contraindications, but also results in occasional adverse reactions and complications.[22,23] Since intrathecal injections rely on catheter pumping devices, they involve a significantly increased infection risk. Moreover, the reported incidence rate of complications ranges from 15% to 40%, which

increases with the extension of the follow-up interval.[24,25] Therefore, stem cell recruitment to the spinal cord is a major impediment to stem cell application to neuropathic pain. Magnetic targeting technology has provided attractive possibilities and was originally developed to optimize chemotherapy procedures. It involves prior MSC magnetization followed by in vivo targeting with the aid of a magnetic field. This allows a larger proportion of the inoculated cells to reach the injured site.[26]

Iron oxide nanoparticles (NPs) in the Fe₃O4 form have been approved for clinical applications due to their remarkable biocompatibility. Superparamagnetic Fe_3O_4 NPs, which are among the most popular magnetic resonance imaging reagents, are widely used in cancer diagnosis.[27] Dopamine (DA), which is among the most important natural neurotransmitters, can spontaneously polymerize under alkaline conditions without needing additional oxidants.[28] Polydopamine (PDA) has excellent biocompatibility and biodegradability. This study aimed to apply Fe_3O_4@PDA composite superparticles with Fe_3O_4 NPs and PDA as core and shell, respectively, which further improved their physiological stability and biocompatibility. This study sought to apply human umbilical cord MSCs. Compared with bone marrow-derived stem cells, human umbilical cord MSCs have shown neurotrophic factor production and a more obvious effect on neuropathic pain.[29] This study aimed to establish Fe_3O_4 @polydopamine(PDA)-labeled mesenchymal stem cells (MSCs); moreover, we aimed to guide MSCs using a magnetic field to the spinal cord segments showing pain-related responses to allow homing and gathering in advance in order to fully employ their repair function. (Figure 1)

Materials and Methods
Preparation of Fe_3O_4@PDA NPs
The following materials were prepared: iron acetylacetonate (Fe(acac)₃, 99.9+%), benzyl ether (99%), 1,2-hexadecanediol (90%), oleylamine (OLA, 70%), oleic acid (OA, 90%), sodium dodecyl sulfate (SDS, 99%), tris(hydroxymethyl) aminomethane (99.0%), and DA hydrochloride (99.0%). The above materials were purchased from Sigma-Aldrich. The experimental method followed is as described in a previous study,[27] and the specific procedural steps can be found in the supplementary Materials. Briefly, Fe_3O_4 NPs were prepared using the thermal decomposition method; subsequently, SDS-capped-Fe_3O_4 NPs were prepared by
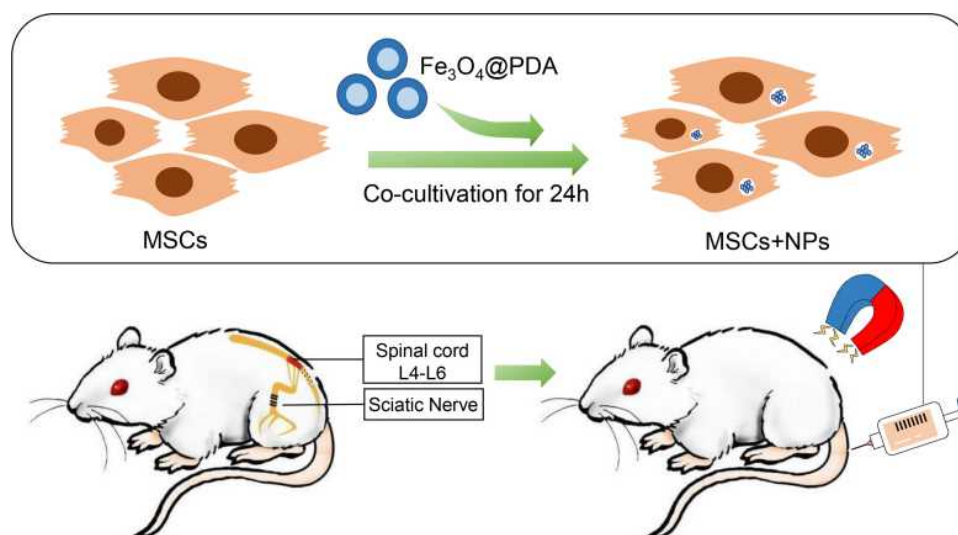
Figure 1 Experimental design: MSCs were labeled using $Fe_3O_4@PDA$. Subsequently, $Fe_3O_4@PDA$-labeled MSCs were injected into the tail vein of rats. The experimental rat was a model of sciatic nerve compression injury; moreover, the pain central response area was the L4-L6 segment of the spinal cord. We applied a regional magnetic field to this segment, which led to the clustering of $Fe_3O_4@PDA$-labeled MSCs in this area.

emulsification, centrifuged, and re-dispersed in Tris buffer (10 mm pH 8.5). Further, some DA monomers were added to make the final concentration of DA 0.3 mg/mL. After stirring at room temperature for 3 h, we obtained PDA-coated Fe_3O_4 NPs. Finally, the product was centrifuged in sterile deionized water to remove excess self-polymerizing DA.[30]

Hemolysis Test

After anesthesia, blood was collected from the abdominal aorta of male Wistar rats into an anticoagulant tube. Fresh blood (2 mL) was collected followed by the addition of phosphate-buffered saline (PBS) to 10 mL. Subsequently, it was centrifuged at 1000 g for 5 min thrice with the supernatant being discarded until it became transparent. Further, 15 mL of PBS was added to resuscitate the red blood cells. Moreover, $Fe_3O_4@PDA$ NPs were diluted using PBS to different concentrations (25, 50, 75, 100, 200 μg/mL, weight of NPs/mL). Deionized water and PBS were used as positive and negative controls, respectively. The cell suspension (0.2 mL) was mixed with the working solution (0.8 mL) and incubated at 37 °C for 4 h; subsequently, it was centrifuged at 1000 g. The supernatant absorbance was measured at 577 nm using a microplate reader (Hercules Bio-Rad Laboratories, California, USA). The hemolysis rate was calculated based on the following test formula:

Hemolysis rate (%) = $[(OD_M-OD_0)/(OD_1-OD_0)] \times 100\%$

where OD_M is the value of each detected concentration on the microplate reader. OD_1 is the positive control and OD_0 is the negative control.

MSCs Isolation and Expansion

The use of the human umbilical cord in this study was approved by the Ethics Committee of the China-Japan Union Hospital of Jilin University with the patient providing written informed consent. The umbilical cord was washed using penicillin-streptomycin (Gibco, Gaithersburg, MD, USA) in a pre-cooled 0.01 mmol/L petri dish; further, the arteries and veins were removed. Next, it was cut into tissue blocks (approximately 5 mm × 5 mm × 5 mm) with each 3 mm spacer being inoculated into a 10 cm petri dish. Subsequently, we added Dulbecco's Modified Eagle Medium (2~3mL) containing 20% fetal bovine serum (Thermo Fisher Scientific, Waltham, MA, USA) followed by culturing the tissue at 37 °C in 5% CO_2. The culture medium was changed twice a week. After treatment for 2 min with 0.05% trypsin and 0.02% EDTA (Sigma-Aldrich Co., St Louis, MO, USA) at 37 °C, the MSCs were sub-cultured under 80% fusion conditions.

Intracellular NPs and Transmission Electron Microscopy

MSCs were cultured to achieve an 80% fusion rate. Different $Fe_3O_4@PDA$ NP concentrations were added to MSC culture plates followed by incubation for 24 h. Next, the cells were washed thrice with PBS and fixed using 4%

paraformaldehyde for 10 min. Subsequently, MSCs were treated based on the instructions of the Prussian blue staining kit (Beijing Solarbio Science & Technology Co., Ltd.). After staining, the NP density in the cells was observed using an inverted optical microscope (Olympus, Tokyo, Japan).

MSCs were co-cultured with Fe_3O_4@PDA NPs at 50ug/mL for 24 h. Next, the cells were digested with trypsin, washed with PBS, and re-suspended thrice. This was followed by centrifuging the cells for 10 minutes at 1000r, discarding the supernatant, adding electron microscope fixative solution, and fixing at 4°C for 24 hours. We determined the ultrastructural characteristics of Fe_3O_4@PDA NPs in cells using transmission electron microscopy (FEI Czech Republic s.r.o, Netherlands).

Flow Cytometry of MSCs Characteristics

To evaluate surface marker expression, we detached MSCs from passage 3 and stained them according to the protocol of the Human MSC Analysis Kit (562245, BD Biosciences, USA). Flow cytometry data (FACSAriaII, BD, USA) were analyzed using FlowJo V10 software.

MSCs Differentiation Potential

To evaluate the differentiation potential, MSCs were inoculated into 12-well plates at a density of $5 \times 10^3/cm^2$ based on the manufacturer's protocol for the differentiation-inducing medium. Based on the human stem cell osteogenesis and adipogenesis differentiation kits (Gibco, Thermo Fisher Scientific, Waltham, MA, USA), MSCs were cultured for 28 and 21 days, respectively. Finally, we used the Alizarin Red and Oil Red O Staining Kit (Shanghai Yuanye Bio-Technology Co., Ltd, China) to detect the osteogenesis and adipogenesis differentiation ability of MSCs loaded with and without Fe_3O_4@PDA NPs.

Viability Study and Proliferation Assessment

We inoculated 5×10^4 MSCs into 96-well plates and cultured them with different concentrations of Fe_3O_4@PDA NPs (0, 25, 50, 75, 100, 200 µg/mL) for 24 h. We added 10 ul CCK-8 solution (Beyotime Biotechnology, China) to each well and incubated it at 37 °C for 2 h. The absorbance at 450 nm was detected using a microplate reader. The test was repeated thrice at each concentration.

We inoculate 5×10^4 MSCs and 5×10^4 Fe_3O_4@PDA-labeled MSCs (50 µg/mL) into 96-well plates, respectively. They were subsequently cultured at 37 °C for 1, 3, 5, and 7 days. Next, 10 ul CCK-8 solution (Beyotime Biotechnology, China) was added to each well and incubated at 37 °C for 2 h. Finally, the absorbance at 450 nm was detected using a microplate reader with triplicate experiments being conducted for each group.

Sciatic Nerve Chronic Compression Injury Model in Rats

We applied the classical model of chronic compression sciatic nerve injury (CCI), which was first described by Bennett and Xie in 1988.[31] Experimental rats were anesthetized by intraperitoneal injection of 3 mg/mL pentobarbital sodium solution (1mL/100g). After shaving and disinfecting the right thigh, the skin was cut and the sciatic nerve was exposed in the middle of the thigh by dissociating the adhesive fascia between the gluteus muscle and biceps femoris. A 4–0 silk thread was loosely ligated four times above the trigeminal section of the sciatic nerve at 1-mm intervals, which caused small and brief convulsions in the muscles around the exposed site. Similar to the CCI group, the sham operation group underwent sciatic nerve exposure but not ligation. Finally, the muscle and skin were sutured using 4–0 and 3–0 silk thread. One person performed all ligation operations.

Animals and Experimental Groups

We randomly divided 60 male Wistar rats (200–220 g) into 5 groups (each group, n = 12). The model was established after one week of animal adaptive breeding; moreover, after 7 days, each treatment group received tail vein injections as follows: the sham operation group (SHAM), saline 1 mL; CCI group (CCI), saline 1 mL; MSC treatment group (MSCs), MSC suspension 1 mL (1×10^6/mL); MSCs+Fe_3O_4@PDA treatment group (MSCs+NPs), MSC-loaded Fe_3O_4@PDA NP suspension 1 mL (1×10^6/mL); MSCs+Fe_3O_4@PDA+Magnet treatment group (MSCs + NPs + M), MSC-loaded Fe_3O_4@PDA NP suspension (1 mL, 1×10^6/mL), with a medical tape being used to fix the magnet (20 mm × 20 mm × 5 mm) at the L4-L6 position of the spinal cord for 24 h. This study was approved by the Animal Welfare and Research Ethics Committee (Experiment number: 20200725–1) and was conducted in accordance with the ethical guidelines of Jilin University. All animal experiments were performed

under the condition of no specific pathogen (SPF) in the animal laboratory.

Fluorescence Imaging of Animals

To trace the localization of MSCs and Fe_3O_4@PDA-labeled MSCs in rats, the cells were collected and stained using CM-Dil cell membrane staining reagent (BestBio, Shanghai, China) in a 15 mL centrifuge tube. After staining, the cells were re-suspended in normal saline at a 1×10^6/mL density and injected into rats. After treatment completion, the rats were decapitated under anesthesia followed by the collection of the heart, liver, spleen, lung, kidney, and spinal cord for fluorescence imaging using an animal fluorescence imager (Caliper Life Science, USA). The excitation and maximum emission wavelengths were 535 nm and 580 nm, respectively.

Behavior Evaluation

A von Frey Hair (North Coast, USA, NC12775-99) was used to evaluate mechanical hyperalgesia. For acclimatization, each rat was separately placed in a customized transparent acrylic chamber ($15 \times 22 \times 15$ cm) with a wire grid at the bottom for 15 min. Subsequently, the "Up and Down" method was used to stimulate the right foot from 2.0 g, with the observation of paw contraction or licking reaction by the rats. Finally, we calculated the mechanical pain threshold as the paw withdrawal threshold (PWT) of each rat.[32]

To evaluate thermal hyperalgesia, a thermal pain meter (BME-410C, China) was used to stimulate the right foot of the rats. The time of foot withdrawal or licking reaction was recorded. Each rat was repeated thrice, with the average time being considered as the thermal withdrawal latency (TWL). To prevent claw tissue damage, we maintained a protective condition with a maximum truncation time of 20 s.

Tissue Preparation and Histological Staining

After treatment, the rats were anesthetized followed by blood sample collection from the abdominal aorta. Subsequently, the rats were decapitated and the spinal cord was retrieved from L4 to L6. A portion of the tissue was quickly frozen in liquid nitrogen for subsequent PCR detection. The remaining tissue was fixed using 4% paraformaldehyde, embedded in paraffin, and cut into 5 μm cross-sections using a microtome. After xylene deparaffinization, reconstituting using graded ethanol, and washing using distilled water, we performed HE and immunohistochemical staining for histological observation. To observe changes in the myelin sheath in the tissues obtained in each rat group, fast blue staining was performed on the spinal cord slices using a Luxol Fast Blue staining kit (Beijing Solarbio Science & Technology Co., Ltd.). The staining results were analyzed using an inverted optical microscope (Olympus, Tokyo, Japan).

For immunofluorescence staining, the spinal cord tissue (L4-L6) was fixed using 4% paraformaldehyde for 24 h; subsequently, it was transferred to 30% sucrose solution for dehydration. Subsequently, the tissue was cut into 8-μm cross-sections using a cryostat, followed by immunofluorescence chemical staining. The staining results were analyzed using an inverted fluorescence microscope (Olympus, Tokyo, Japan).

Quantitative Reverse Transcription PCR and ELISA

The L4-L6 spinal cord was extracted followed by grindings of the tissue. The tissue was digested using TRIzol reagent (Takara Bionics, Kusatsu, Japan) followed by total RNA extraction. The cDNA was synthesized as per the instructions of the PrimeScript™ RT reagent Kit (Takara BioInc, Kusatsu, Japan). Real-time quantitative polymerase chain reaction was performed using TB Green® Premix Ex Taq™ II for relative quantification of glial fibrillary acidic protein (GFAP), C-FOS, and ionized calcium binding adapter molecule-1 (IBA-1) mRNA transcription. The primer sequences used for the above genes are listed in Table 1.

We obtained serum from all rats to measure interleukin-6 (IL-6), interleukin-10 (IL-10), and transforming growth factor-β (TGF-β) levels according to the manufacturer's instructions (MEIMIAN, China). Each sample was tested in triplicate. The absorbance at 450 nm was measured using a microplate reader.

Statistical Analysis

Data analysis and image production were performed using GraphPad Prism 8. The data were expressed as the average and standard error. Between-group comparisons of behavioral data were performed using two-way ANOVA, followed by Tukey's multiple comparisons test. Other data were analyzed using a one-way analysis of variance. Statistical significance was set at $p < 0.05$.

Table 1 Primer Sequences and Product Sizes

Symbol	Primer Sequence	Product Size (bp)
IBA-1	F-GCTGGAGAAACTTGGGGTTCCC R-AACGTCTCCTCGGAGCCACTG	84
GFAP	F-GCGAGCGTGCGGAGATGATG R-CAGTTTGGTGGGCTCCTTGGC	134
c-Fos	F-GCAGCCCACTCTGGTCTCCTC R-GCCGCCTGACATGGTCTTCAC	124
β-actin	F-TCCCTGTATGCCTCTGGTCG R-GTGGTGGTGAAGCTGTAGCC	188

Results and Discussion

Preparation of Fe_3O_4@PDA and Fe_3O_4 @PDA-Labeled MSCs

We synthesized Fe_3O_4@PDA using the aforementioned method. In our previous study, we carried out a detailed physical and chemical characterization of the particle.[27] First, the NP morphology was characterized through transmission electron microscopy, as shown in Figure 2C. The NPs were spherical (diameter: 55 nm–60 nm); moreover, the PDA was uniformly wrapped on the surface of the naked Fe_3O_4 core. Previous studies confirmed that Fe_3O_4 nanoparticles are superparamagnetic, and the self-

assembly and PDA coating process of NPs did not affect the original superparamagnetic behavior.[27] Contrastingly, the formation of a spherical self-assembly structure improved the performance of inorganic NPs based on the collective effect.[33,34] To reconfirm the Fe_3O_4@PDA magnetism, Fe_3O_4@PDA NPs were uniformly dispersed in saline with magnets being placed on one side (Figure 2A). After 24 h, the NPs were attracted to the magnet side with the saline returning to being clear.

Given the excellent biocompatibility and biodegradability of PDA, Fe_3O_4@PDA could be easily swallowed into cells. After culturing MSCs in the medium containing Fe3O@PDA NPs for 24 h, we obtained Fe_3O_4@PDA-labelled MSCs. Transmission electron microscopy (Figure 2D) revealed the presence of Fe_3O_4@PDA in the endocytosis vesicles of MSCs. As shown in Figure 2B, Fe_3O_4@PDA-labeled MSCs are brownish-black. Given the partial NP aggregation in the cells and the large cell diameter, the cells can be attracted to one side by magnets after 15 min. This further indicated the good magnetic properties of Fe_3O_4@PDA-labeled cells.

The Optimal Concentration of Fe_3O_4 @PDA for Labeling MSCs is 50 μg/mL

Toxicity accounts for 20% of all drug failures in clinical trials; specifically, the effect on the blood system accounts
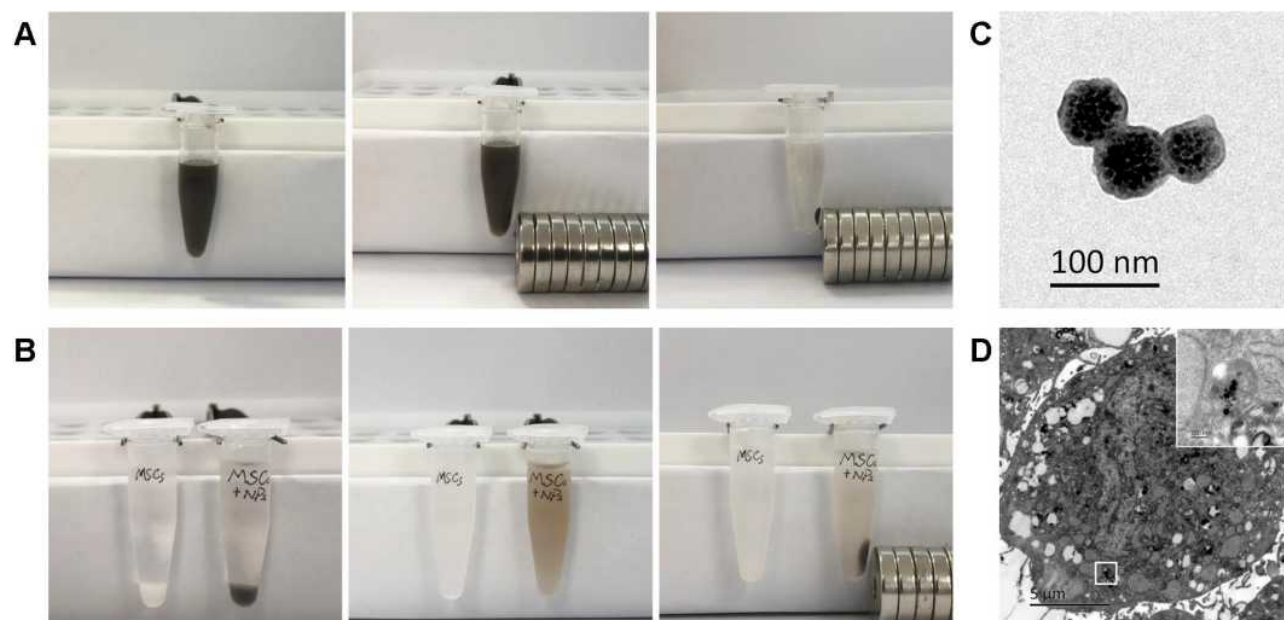

Figure 2 Morphological and magnetic characteristics of Fe_3O_4@PDA NPs and Fe3O4@PDA-labelled MSCs. (**A**) In the physiological saline suspension of Fe_3O_4@PDA, the materials were attracted to the magnet side after 24 hours. (**B**) Saline suspension of MSCs and Fe_3O_4@PDA-labeled MSCs, the Fe_3O_4@PDA labeled MSCs was attracted to the magnet side at 15 min after placing the magnet. (**C**) Transmission electron microscope image of Fe_3O_4@PDA. (**D**) Transmission electron microscope image of Fe_3O_4 @PDA-labeled MSCs (scale: 5 μm) and Fe_3O_4@PDA in endocytosis vesicles (scale: 200 nm).

for 11% of all drug abstinence reported by the FDA.[35,36] We performed a hemolysis test in vitro, which is considered a reliable and effective method for confirming the blood compatibility of nanomaterials (Figure 3A). Even after 4 hours of incubation, Fe_3O_4@PDA NPs did not induce significant hemolysis at a concentration of 25, 50, and 75 μg/ mL, with respective hemolysis rates being 1.02%, 1.06%, and 4.51%, respectively, which was within the acceptable 5% hemolysis threshold (Figure 3B). The results showed that within a certain range, Fe_3O_4@PDA did not result in hemolysis in vitro and that it had certain blood compatibility.

We explored the efficiency of NPs entering MSCs through Prussian blue staining. As shown in Figure 3C, cytoplasmic Fe_3O_4@PDA was seen as typical blue. The five different concentrations tested could produce good markers for stem cells; moreover, stem cell uptake of the material was positively correlated with its concentration. To achieve a satisfactory labeling rate and avoid the effect of phagocytosing extra materials on cell activity, the suitable material concentration is 50 and 75 μg/mL.

Additionally, we used the CCK8 method to detect the effect of different Fe_3O_4@PDA concentrations on MSC activity. Figure 3D shows the experimental results of survivability 24 hours after 25, 50, 75, 100, and 200

μg/mL Fe_3O_4@PDA-labeled MSCs. Compared with the blank control group, there was no significant change in cell viability when the Fe_3O_4@PDA concentration was < 50 μg/mL. NPs for MSC labeling based on cell therapy should not impair MSC survival and proliferation. Based on the aforementioned experimental results, we finally selected a concentration of 50 μg/mL, which achieved a satisfactory labeling rate, good blood compatibility, and retained ≥ 95% cell vitality for further experiments.

Fe_3O_4@PDA Does Not Affect MSC Characteristics, Differentiation, and Proliferation

After determining the best labeling concentration for MSCs, we further studied whether the material affected the MSC characteristics. First, the cultured adherent cells presented the morphological characteristics of MSC fibroblasts. We analyzed the typical surface markers of stem cells through flow cytometry. In 2006, the International Society of Cell Therapy proposed that MSCs were positive for CD73, CD90, and CD105; however, they were negative for CD34, CD45, CD11b, CD14, CD19, CD79 α, and HLA-DR. Further, it is known that MSCs express
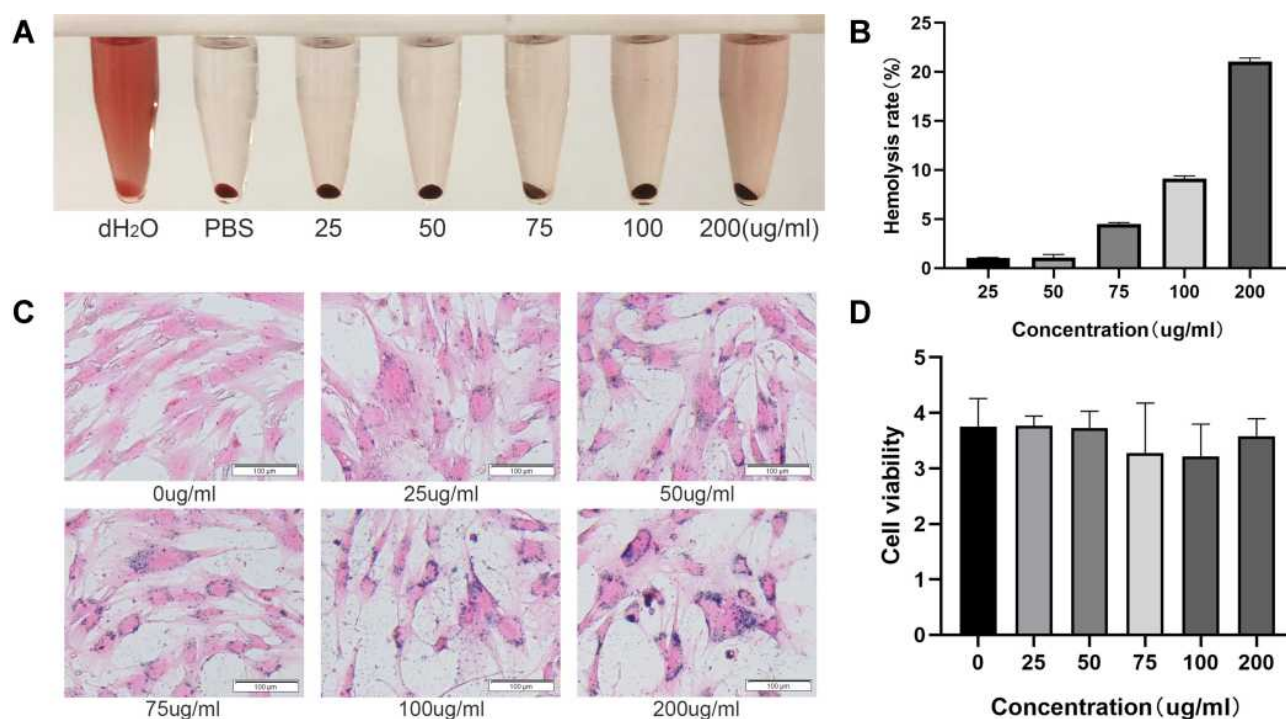

Figure 3 Determination of the optimal labeling concentration of Fe_3O_4@PDA NPs. (**A**) The supernatant was obtained by incubating different concentrations of Fe_3O_4@PDA NPs in diluted fresh red blood cells. (**B**) Hemolysis rate resulting from different concentrations of Fe_3O_4@PDA NPs. (**C**) MSC staining results using Prussian blue iron staining kit, scale 100 μm. (**D**) The cell proliferation activity of different concentrations of NPs (0,25,50,75,100,200 μg/mL).

numerous cell surface markers, including CD44, CD29, CD200, CD166, CD146, and CD271.[36,37] Figure 4A presents our results. Both MSCs and NP-labeled MSCs strongly express typical surface antigens (CD73, CD90, CD105, and CD44); moreover, they are negative for surface antigens not found in stem cells (negative MSC cocktail: CD45, CD34, CD11b, CD19, and HLA-DR). There was no significant between-group difference, which indicated that using Fe_3O_4@PDA did not alter the expression of characteristic surface markers of MSCs.

Next, we cultured MSCs and Fe3O4@PDA-labelled MSCs in a medium for promoting adipogenesis and osteogenic lineage. As shown in Figure 4B, both MSC groups showed similar differentiation into two lineages with the marked formation of adipoblasts and osteoblasts. There were no differences in Fe_3O_4@PDA-labeled MSCs between

osteogenic and adipogenic controls; specifically, Fe_3O_4 @PDA did not affect the differentiation potential of stem cells.

Finally, we applied the CCK-8 method to detect Fe_3O_4 @PDA-labeled MSC proliferation for 7 d (50 μg/mL). Fe_3O_4@PDA not only did not inhibit MSC proliferation, but also showed a slight promoting effect on cell proliferation on the 3rd, 5th, and 7th day (Figure 4C). This finding exceeded our expectations. Numerous studies have reported that different nanomaterials can promote cell proliferation, which may involve intracellular signal transduction, altering protein expression, and regulating cell function.[38,39]

Taken together, the Fe_3O_4@PDA-labeled MSCs we obtained retained distinctive stem cell characteristics; moreover, Fe_3O_4@PDA did not alter their differentiation potential and proliferation ability and were suitable for the next cell therapy.
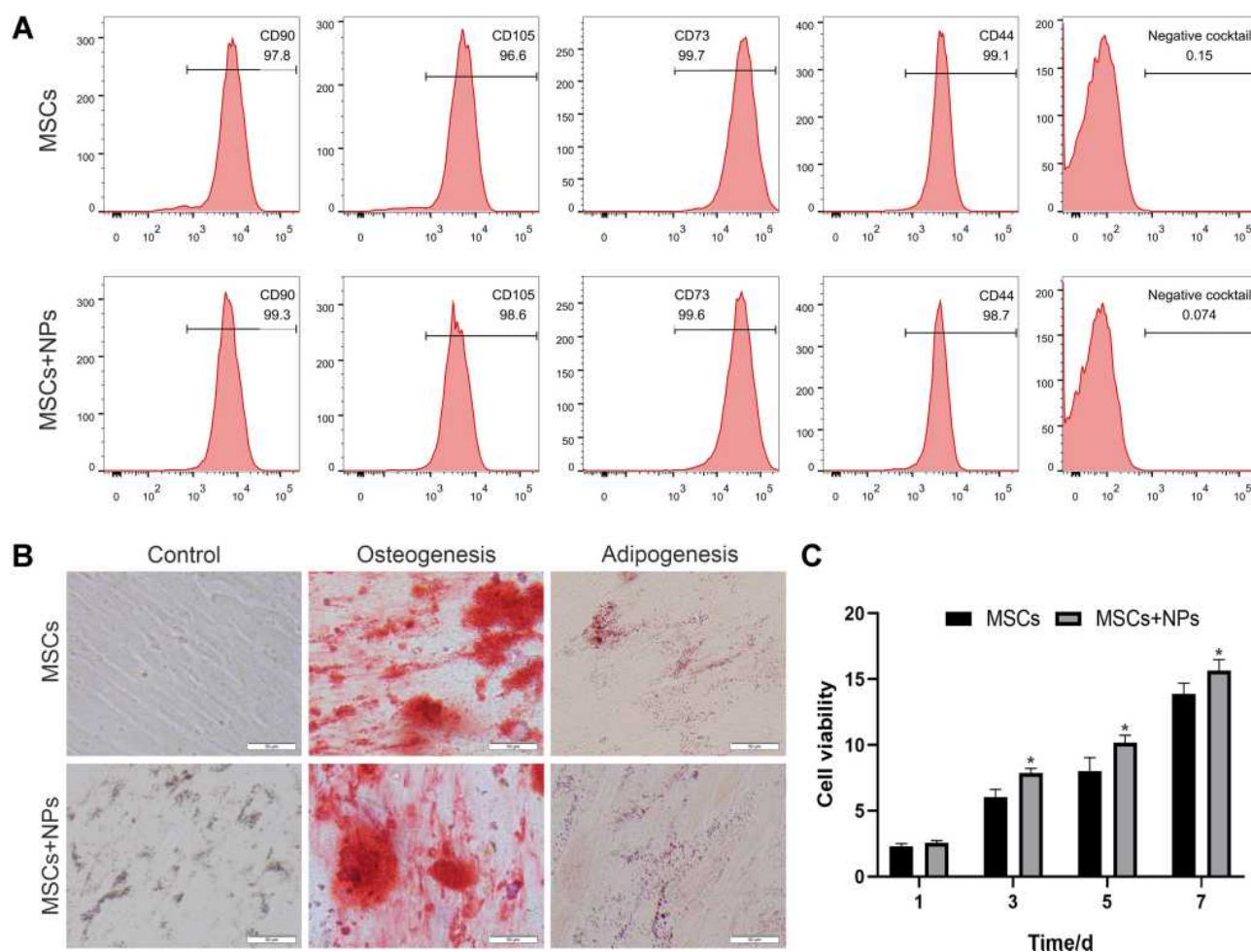

Figure 4 The effect of 50 μg/mL NPs on the MSC characteristics. (**A**) Fluorescence-activated cell sorting analysis of labeled MSCs revealed strong expression of typical surface antigens of stem cells, including CD90, CD105, CD73, and CD44; contrastingly, it was negative for surface antigens not contained in stem cells (negative cocktail: CD45, CD34, CD11b, CD19, and HLA-DR). (**B**) Both MSCs and Fe_3O_4@PDA-labeled MSCs differentiated into osteoblasts and adipocytes. (**C**) MSC labeled using 50 μg/mL Fe_3O_4@PDA NPs proliferated for 1, 3, 5, and 7 days.*$P<0.05$.

Fe₃O₄@PDA-Labeled MSCs Attenuate CCI-Induced Hyperalgesia and Allodynia in Rats

Our rats showed thermal hyperalgesia and mechanical abnormal pain within 1 post-CCI week (PWT and TWL were significantly lower than those in the sham operation group) (Figure 5A and B), with this phenomenon continuing throughout the experiment. The sham group did not show mechanical abnormal pain or thermal hyperalgesia.

Moreover, there was no significant difference in body weight gain in each group during the whole experiment (Figure 5C).

We administered the corresponding cell therapy on the eighth post-CCI day. As shown in Figure 5A, the PWT of the three treatment groups slightly increased on the post-treatment day 1; however, there was no significant difference between the three MSC + NP + M group and the CCI group. On post-treatment day 7, the PWT was significantly higher in the MSC + NP +M group than in the CCI group
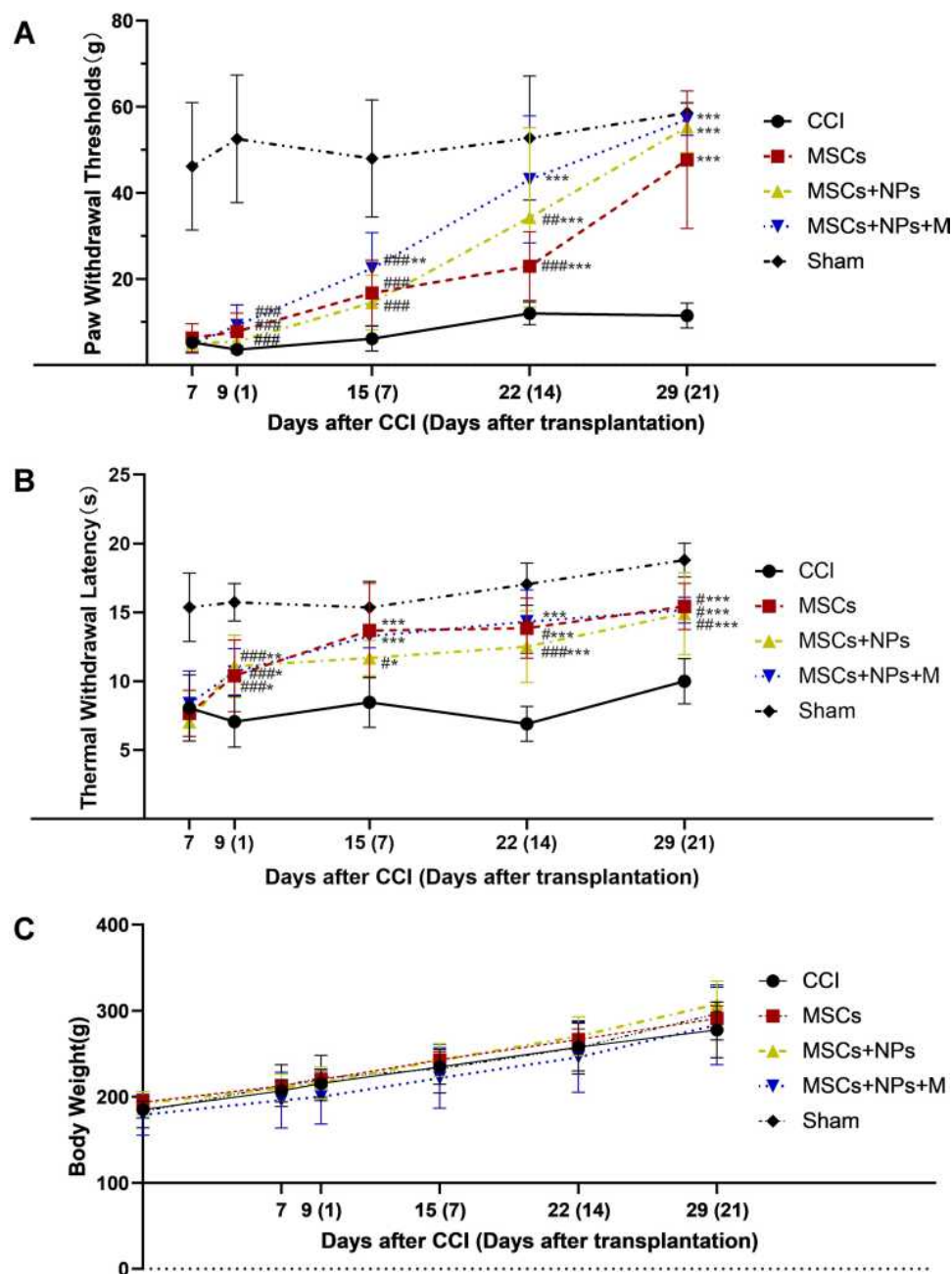
Figure 5 Treatment effects on behavior and body weight in each group. (**A**) Changes of mechanical paw withdrawal threshold of rats; (**B**) Changes in the thermal withdrawal latency of rats; (**C**) Changes in the body weight of rats. Compared with SHAM group, #P < 0.05, ##P < 0.01, ###P < 0.001; compared with CCI group, *P < 0.05, **P < 0.01, ***P < 0.001.

(P = 0.0056). On the 14th treatment day, there was no significant difference between the MSC + NP + M and SHAM groups. After 21 treatment days, there were good therapeutic effects in the MSC, MSC + NP, and MSC + NP +M groups; however, there was no significant difference in the PWT between the MSCs+ NP +M and SHAM groups. Based on these results, we believe that the combined action of an external magnetic field and intracellular Fe_3O_4@PDA accelerates MSC homing, which facilitates more effective MSC gathering in the L4-L6 spinal cord region; moreover, it plays a better role in advance.

However, our findings are inconsistent with the expected results. As shown in Figure 5B, there was a significant increase in the TWL of the three treatment groups ($P_{MSCs} = 0.021$, $P_{MSCs+NPs} = 0.003$, $P_{MS\ Cs+NPs+M} = 0.014$) at one post-treatment day; however, there was no significant among-group differences in the following time. There was no significant among-group difference in the therapeutic effect. TWL is a good indicator of heat allodynia and hyperalgesia. Thermal hyperalgesia is especially prominent in inflammatory diseases; further, its mechanism is mainly C fiber sensitization and A δ fiber block in neuropathic pain. Thermal hyperalgesia is mainly caused by peripheral mechanisms; however, it exists in 10% of patients with central involvement.[40,41] In this study, since we injected cells into the tail vein, some of the MSCs without magnetic targeting were homed to the injured sciatic nerve and exerted the anti-inflammatory effect of stem cells in the peripheral circulation. Consequently, it equalized the therapeutic effect of the three groups on thermal hyperalgesia.

Fe_3O_4@PDA-Labeled MSCs Reached the Spinal Cord Earlier Under Magnetic Targeting

To confirm that the cells targeted the spinal cord, we performed fluorescence tissue imaging of the rats. Before the cell injection, all the cells were labeled using a fluorescent dye; moreover, the labeled cells showed stable red fluorescence. Moreover, the main organs underwent fluorescence imaging on the 1st and 7th post-injection day. Previous studies have reported that stem cell injection into the caudal vein leads to most of the cells being trapped in the lungs.[21] Figure 6A presents the main stem cell distribution in organs on the day after cell injection. In the MSC group and MSC + NP group, some MSCs were targeted to the spinal cord while others remained in the lung. Contrastingly, in the MSC + NP + M group, MSCs had almost been completely excreted from the lung. Seven days after cell injection, all MSCs were excreted from the lungs in all three treatment groups; however, the MSC + NP +M group showed a wider fluorescence range, which indicated that more MSCs were gathered (Figure 6B). Simultaneously, the corresponding
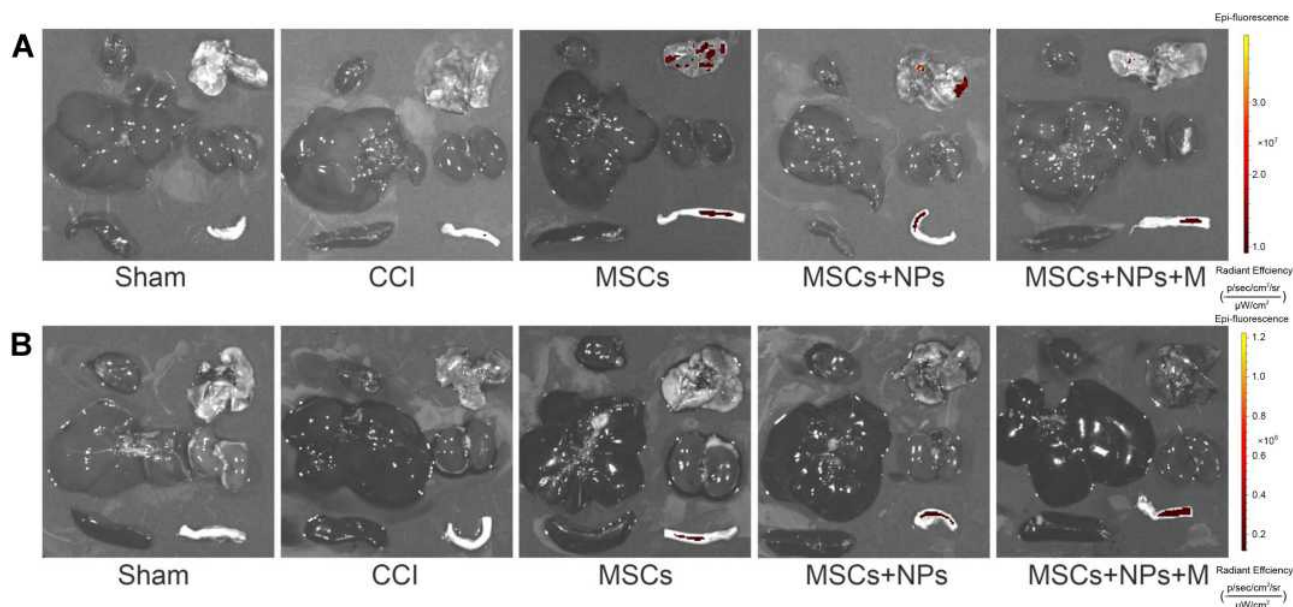

Figure 6 Fluorescence imaging of the animal organs. (**A**) Fluorescence distribution in the organs at 24 post-injection hours. (**B**) Fluorescence distribution in the organs at seven post-injection days. Organs order: Left, from top to bottom: the heart, liver, and spleen; right, from top to bottom: the lung, kidney, and spinal cord.

frozen spinal cord sections were examined; however, there were no positive red cells (Supplementary Figure S1). Some studies have shown that stem cells can reach the brain-injury site through the blood-brain barrier. However, the extent and mechanism of the bone marrow MSCs actively crossing the blood-brain barrier are not clear. In the study of Park et al, a small number of radiolabeled stem cells were found in the brain of animal models of Alzheimer's disease by intravenous injection of MSCs.[42] However, in the study of stem cell homing conducted by Sackstein et al, bone marrow MSCs had the least binding to endothelial cells and could only moderately infiltrate into the bone marrow.[43] This contradicts the possible mechanism of stem cells penetrating the blood-brain barrier.[44] In this study, we are not certain whether the MSCs did not penetrate the spinal cord parenchyma through the blood-brain barrier, or whether the process of penetrating the blood-brain barrier led to the loss of cell membrane fluorescence. The fluorescence obtained may be due to the stem cell enhancement on the surface of the spinal cord. Similar results in studies of stem cells such as Teng in the treatment of neuralgia were achieved. Teng et al believe that the MSCs do not act locally or directly penetrate the spinal cord neurons, and there should be an intermediary step in the mechanism of relieving neuropathic pain, which could be achieved by releasing the intracellular contents of the MSCs.[45]

MSCs Reduces Demyelination and c-Fos Expression in the Spinal Cord

Nerve injuries, including excitotoxicity, oxidative stress, and inflammation, induce nerve fiber degeneration and myelin loss.[46,47] This study used LFB staining to evaluate the structural integrity of myelin in the spinal cord after three treatment weeks. As shown in Figure 7A, myelin shows a blue substrate reaction in the transverse spinal cord section. In the SHAM group, there was a dense and regularly arranged blue color. Contrastingly, in the CCI group, the LFB staining decreased with a sparse arrangement. Compared with the CCI group, there was increased LFB staining in the MSC, MSC + NP, and MSC + NP +M groups. The MSC + NP +M group showed the best reduction in spinal cord demyelination, which was similar to that in the SHAM group. The results showed that magnetic action facilitated the accumulation of the Fe₃O₄@PDA-labeled MSCs in the spinal cord, which allowed better treatment using MSCs.

We performed immunohistochemical staining for c-Fos in the spinal dorsal horn. C-Fos, which is a protein product of the immediate-early gene c-Fos, is a marker for nociceptive neuron activation in the spinal cord and medulla oblongata dorsal horn.[48,49] C-Fos may be a molecular marker for evaluating neuropathic pain. As shown in Figure 7B, compared with the SHAM group, there was a significant increase in c-Fos expression in the CCI group and a decrease in the MSC, MSC + NP, and MSC + NP +M groups. The MSC + NP + M group showed the most significant inhibition of c-Fos expression. PCR analysis of the L4-L6 spinal cord confirmed the significant inhibition of c-Fos expression in the MSCs+ NP +M group (Figure 7C). These findings are further indicative of the role of magnets and Fe₃O₄@PDA in improving MSC homing.

Changes in Serum Inflammatory Factors IL-6, IL-10, and TGF- β

Several studies have reported that stem cells can reduce the levels of pro-inflammatory factor IL-6 and increase the anti-inflammatory factor IL-10 for exerting an analgesic effect on NP.[50–52] TGF β is an important regulator of central sensitization, which attenuates glutamate-induced excitotoxic neuronal damage in a concentration-dependent manner.[53] Intrathecally injected stem cells release TGF-β in the cerebrospinal fluid, which reduces the increase in neuronal excitability after nerve injury, and thus exerts an analgesic effect.[21] We detected the changes of IL-6, IL-10, and TGF- β in serum of rats in each group following three weeks of treatment with ELISA kit. (Figure 7F–H,) We found that compared with the SHAM group, serum IL-6 increased and IL-10 and TGF-β decreased in the CCI group, and the difference was statistically significant (P_{IL-6}=0.022, P_{IL-10}=0.008, $P_{TGF-β}$ = 0.034). The MSCs group decreased with the increase of serum IL-6 caused by CCI, Purge 0.022, while in the MSCs+NPs group and the MSCs+NPs +M group, the IL-6 also decreased compared with the CCI group.(Figure 7F); however, we did not calculate the statistical difference. The serum IL-10 of the three treatment groups seemed to be higher than that of the CCI group, but there was no statistically significant difference between the MSCs group and the CCI group; however, it is noteworthy that there was no significant difference in the IL-10 level between the MSCs group.(Figure 7G), the MSCs+NPs group, and the SHAM group. There was no
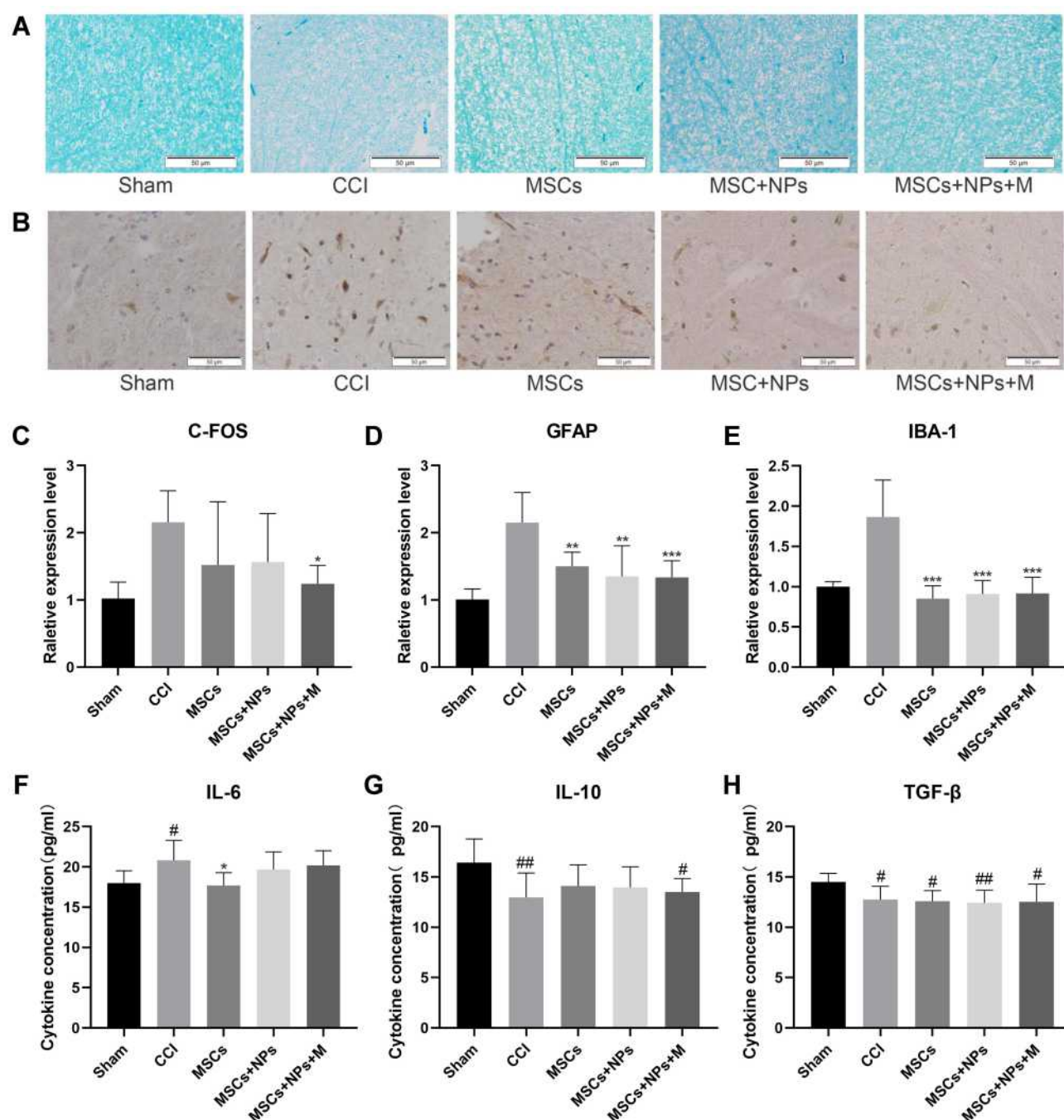
Figure 7 Effect of each group on protein and factor expression in the spinal cord and serum. (**A**) The transverse spinal cord section was stained through LFB staining; moreover, the image was shown in the right dorsal horn of the spinal cord. Myelin showed a blue substrate reaction in the section. (**B**) Immunohistochemical staining of c-Fos in the transverse section of the spinal cord revealed that the image site was the right dorsal horn of the spinal cord. Positive cells were stained dark brown. (**C–E**) We used qRT PCR to detect spinal cord expression of c-Fos, GFAP, and IBA-1 mRNA. Compared with CCI group,*$P < 0.05$, **$P < 0.01$, ***$P < 0.001$. (**F–H**) Detection of serum IL-6, IL-10, and TGF- β using an ELISA kit. Compared with SHAM group, #$P < 0.05$, ##$P < 0.01$; compared with CCI group, *$P < 0.05$.

significant change in the serum TGF- β in each group. (Figure 7H).

Here we speculate that since the cells in this study were injected through the tail vein, the MSCs had an anti-inflammatory effect on the CCI and reduced the level of IL-6 in serum. At the same time, the anti-inflammatory

factor IL-10 in the serum of the three treatment groups seemed to be higher than that of the CCI group, but there was no statistical difference between the MSCs group and the CCI group; however, there was still a difference between the MSCs+NPs+M group and the SHAM group, indicating that the peripheral role of the MSCs+NPs+M

group was the weakest. This also demonstrates that since the cells are targeted to the spinal cord in the MSCs+NPs +M group, the treatment of neuropathic pain is achieved through a central mechanism, and there is no significant change in the inflammatory factors in peripheral blood. TGF-β is an important regulatory factor against central sensitization, which plays an analgesic role through the regulation of the central mechanism. This is also consistent with our results.

Accelerating MSC Homing to the Spinal Cord Can Allow Earlier Inhibition of IBA-1 and GFAP Expression

After nerve injury, microglia are activated within 24 h; moreover, astrocytes are activated soon after nerve injury, lasting for 12 weeks. Subsequently, astrocytes and microglia release cytokines and induce a series of cellular responses, resulting in spinal cord excitement and neuroplastic changes, which are closely associated with neuropathic pain occurrence.[54,55] Several studies have reported that stem cells can effectively inhibit glial cell activation.[12,56–58] Therefore, we used PCR to detect mRNA expression of the microglial marker (IBA1) and astrocyte marker (GFAP) in the spinal cord after three treatment weeks. As shown in Figure 7D and E, the MSC, MSC + NP, and MSC + NP +M groups showed a significant decrease in the CCI-induced expression of IBA-1 and GFAP. There was no significant among-group difference in IBA-1 expression; however, there was a more significant decrease in GFAP in the MSC + NP + M group (P < 0.001). Consistent with previous findings, the synergistic effect of the magnetic field and Fe_3O_4@PDA allowed MSCs to reach the spinal cord faster and exert a better therapeutic effect. We collected the spinal cord of rats one day after cell injection and performed immuno-fluorescence staining. Figure 8 shows the early changes in GFAP and IBA-1 levels in the spinal dorsal horn after 24 h of treatment. After 24 h of treatment, there was no significant difference in the fluorescence intensity and the number of GFAP positive cells among the MSC, MSC + NP, and CCI groups; however, there was a significant decrease in the fluorescence intensity and number of positive cells in the MSC + NP + M group (Figure 8A and C). However, there were among-group differences in the post-treatment IBA-1 alterations after

24 h. Compared with the CCI group, the MSC and MSC + NP groups showed inhibited microglia expression in just one day; further, there was a more significant inhibitory effect in the MSC + NP + M group (Figure 8B and D). Fe_3O_4@PDA-labeled MSCs could prematurely inhibit IBA-1 and GFAP expression under the action of a magnetic field and quickly play a role in the therapeutic effect.

Fe_3O_4@PDA NPs Have No Significant Toxicity to the Main Organs of Rats

We collected the main organs of the rats after three treatment weeks and performed HE staining to evaluate the potential toxicity of Fe_3O_4@PDA. As shown in Figure 9A, compared with the control group, the treatment groups showed no significant morphological changes in the heart, liver, spleen, lungs, and kidneys. Further, we weighed the main organs and obtained the corresponding organ coefficient compared with the bodyweight; there was no significant among-group difference in the organ-to-body ratio (Figure 9B). These results further indicate the low toxicity of Fe_3O_4@PDA NPs in vivo.

Conclusion

In this study, we successfully obtained Fe_3O_4@PDA and internalized it with MSCs. The resulting Fe3O4@PDA-labelled MSCs showed no change in the stem cell characteristics; moreover, it was magnetic and its movement could be affected by the external magnetic field. Currently, the low efficiency of stem cell recruitment to the spinal cord is a significant impediment to stem cell application in neuropathic pain. We injected Fe_3O_4@PDA-labelled MSCs into animals through the tail vein. Attracted by the magnetic field, Fe_3O_4@PDA-labelled MSCs further and rapidly gathered to the spinal cord. This improved the use of the MSC repair function, which enhanced the treatment efficiency and effect. Our findings are indicative of the safety and feasibility of injecting labeled MSCs into clinically related animal models for treating neuropathic pain. Moreover, they provide a reference for the future application of stem cells in patients with clinical neuropathic pain.
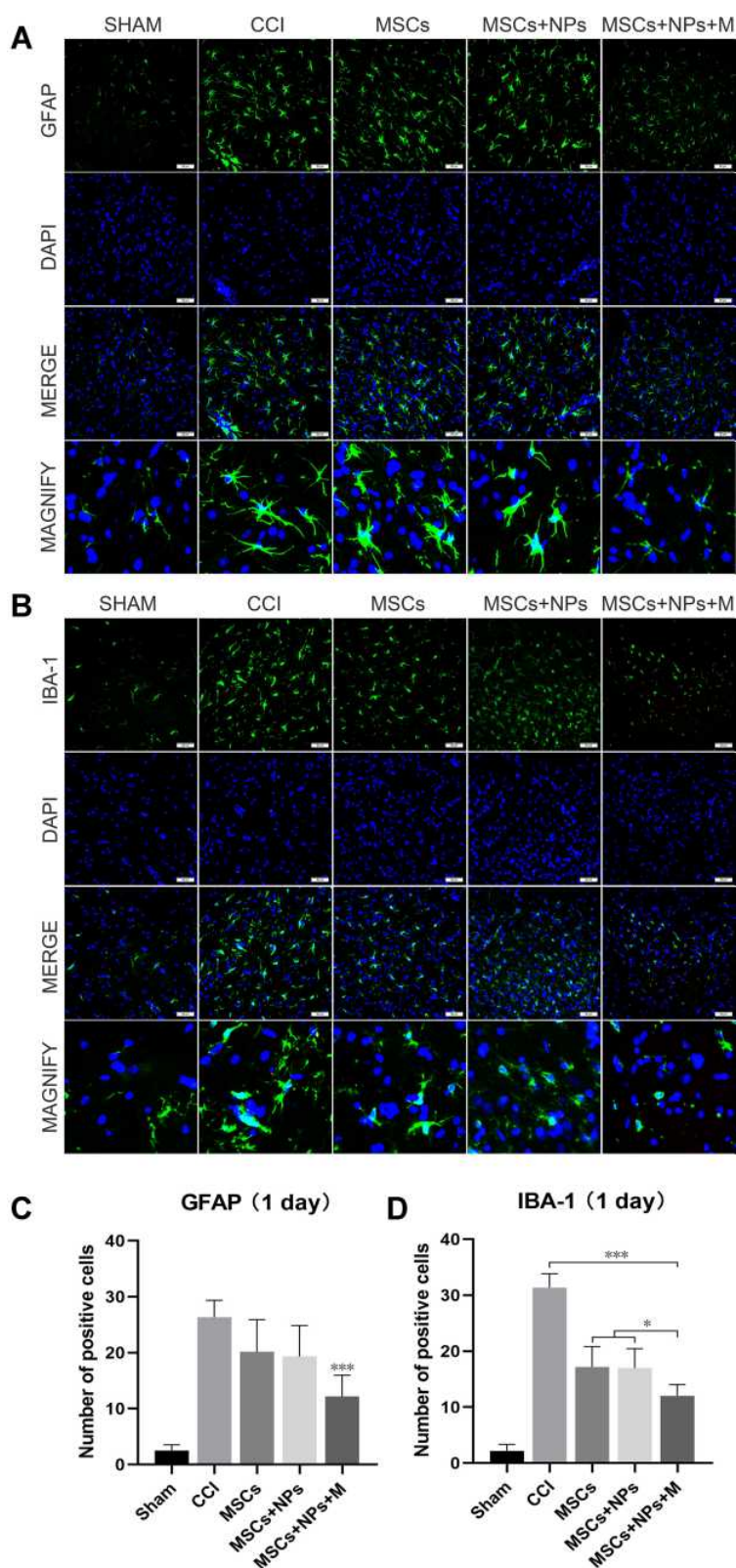
Figure 8 Immunofluorescence showing the changes in activation of spinal cord astrocytes and microglia from different treatment groups after one day of treatment. (**A**) Changes in astrocyte marker GFAP; (**B**) Changes in microglial marker IBA-1. The picture shows the right dorsal horn of the spinal cord on a scale of 50 μm. (**C**) Number of positive cells of GFAP. Compared with CCI group, ***P < 0.001. (**D**) Number of positive cells of IBA-1. Compared with CCI group,*P < 0.05, ***P < 0.001.
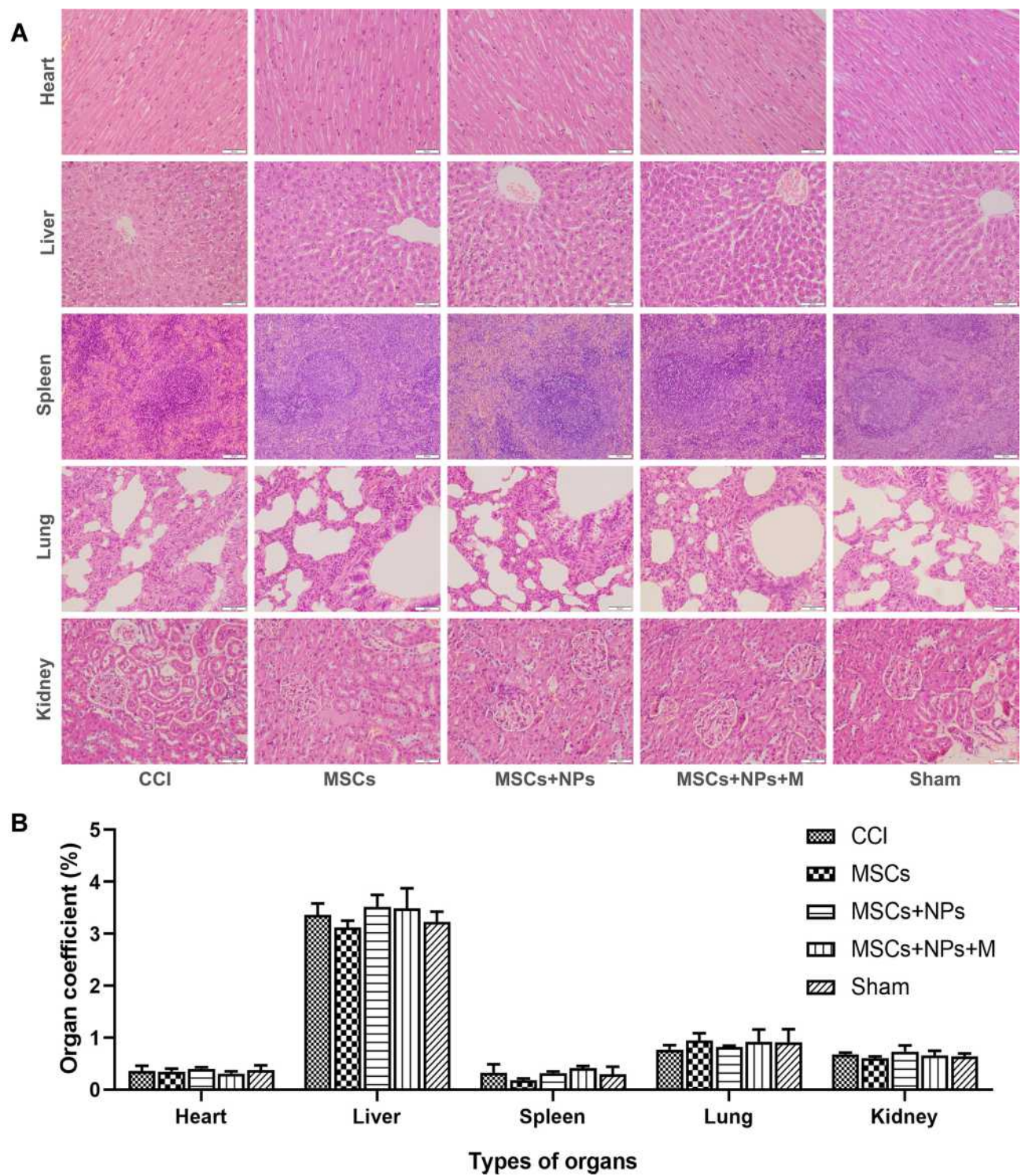
Figure 9 Effects of materials on the main organs of rats after three treatment weeks. (**A**) Hype staining of the heart, liver, spleen, lungs, and kidneys in each group. The scale is 50 μm. (**B**) The changes in the organ coefficients of the heart, liver, spleen, lungs, and kidneys in each group.

Data Sharing Statement

The datasets used or analysed during the current study are available from the corresponding author on reasonable request.

Ethics Approval and Consent to Participate

Acknowledgments

Author Contributions

All authors made a significant contribution to the work reported, whether that is in the conception, study design, execution, acquisition of data, analysis and interpretation, or in all these areas; took part in drafting, revising or critically reviewing the article; gave final approval of the version to be published; have agreed on the journal to which the article has been submitted; and agree to be accountable for all aspects of the work.

Funding

Disclosure

The authors declare that they have no competing interests.

References

1. Treede RD, Rief W, Barke A, et al. Chronic pain as a symptom or a disease: the IASP classification of chronic pain for the international classification of diseases (ICD-11). *Pain*. 2019;160(1):19–27. doi:10.1097/j.pain.0000000000001384
2. Bouhassira D. Neuropathic pain: definition, assessment and epidemiology. *Rev Neurol*. 2019;175(1–2):16–25. doi:10.1016/j.neurol.2018.09.016
3. van Hecke O, Austin SK, Khan RA, et al. Neuropathic pain in the general population: a systematic review of epidemiological studies. *Pain*. 2014;155(4):654–662. doi:10.1016/j.pain.2013.11.013
4. Zilliox LA. Neuropathic pain. *Continuum (Minneap Minn)*. 2017;23 (2):512–532. doi:10.1212/CON.0000000000000462
5. Torrance N, Smith BH, Bennett MI, et al. The epidemiology of chronic pain of predominantly neuropathic origin. Results from a general population survey. *J Pain*. 2006;7(4):281–289. doi:10.1016/j.jpain.2005.11.008
6. Dworkin RH, Panarites CJ, Armstrong EP, et al. Is treatment of postherpetic neuralgia in the community consistent with evidence-based recommendations? *Pain*. 2012;153(4):869–875. doi:10.1016/j.pain.2012.01.015
7. Torrance N, Smith BH, Watson MC, et al. Medication and treatment use in primary care patients with chronic pain of predominantly neuropathic origin. *Fam Pract*. 2007;24(5):481–485.
8. Torrance N, Ferguson JA, Afolabi E, et al. Neuropathic pain in the community: more under-treated than refractory? *Pain*. 2013;154 (5):690–699. doi:10.1016/j.pain.2012.12.022
9. Hosseini M, Yousefifard M, Aziznejad H, et al. The effect of bone marrow-derived mesenchymal stem cell transplantation on allodynia and hyperalgesia in neuropathic animals: a systematic review with meta-analysis. *Biol Blood Marrow Transplant*. 2015;21 (9):1537–1544. doi:10.1016/j.bbmt.2015.05.008
10. Klass M, Gavrikov V, Drury D, et al. Intravenous mononuclear marrow cells reverse neuropathic pain from experimental mononeuropathy. *Anesth Analg*. 2007;104(4):944–948. doi:10.1213/01.ane.0000258021.03211.d0
11. Lin CR, Wu PC, Shih HC, et al. Intrathecal spinal progenitor cell transplantation for the treatment of neuropathic pain. *Cell Transplant*. 2002;11(1):17–24. doi:10.3727/096020198389744
12. Watanabe S, Uchida K, Nakajima H, et al. Early transplantation of mesenchymal stem cells after spinal cord injury relieves pain hypersensitivity through suppression of pain-related signaling cascades and reduced inflammatory cell recruitment. *Stem Cells*. 2015;33 (6):1902–1914. doi:10.1002/stem.2006
13. Cho KJ, Trzaska KA, Greco SJ, et al. Neurons derived from human mesenchymal stem cells show synaptic transmission and can be induced to produce the neurotransmitter substance P by interleukin-1 alpha. *Stem Cells*. 2005;23(3):383–391. doi:10.1634/stemcells.2004-0251
14. Bae JS, Han HS, Youn DH, et al. Bone marrow-derived mesenchymal stem cells promote neuronal networks with functional synaptic transmission after transplantation into mice with neurodegeneration. *Stem Cells*. 2007;25(5):1307–1316. doi:10.1634/stemcells.2006-0561
15. Puissant B, Barreau C, Bourin P, et al. Immunomodulatory effect of human adipose tissue-derived adult stem cells: comparison with bone marrow mesenchymal stem cells. *Br J Haematol*. 2005;129 (1):118–129. doi:10.1111/j.1365-2141.2005.05409.x
16. Nauta AJ, Fibbe WE. Immunomodulatory properties of mesenchymal stromal cells. *Blood*. 2007;110(10):3499–3506. doi:10.1182/blood-2007-02-069716
17. Franchi S, Castelli M, Amodeo G, et al. Adult stem cell as new advanced therapy for experimental neuropathic pain treatment. *Biomed Res Int*. 2014;2014:470983. doi:10.1155/2014/470983

18. Mazzini L, Mareschi K, Ferrero I, et al. Mesenchymal stromal cell transplantation in amyotrophic lateral sclerosis: a long-term safety study. *Cytotherapy.* 2012;14(1):56–60. doi:10.3109/14653249.2011.613929

19. Hare JM, Traverse JH, Henry TD, et al. A randomized, double-blind, placebo-controlled, dose-escalation study of intravenous adult human mesenchymal stem cells (prochymal) after acute myocardial infarction. *J Am Coll Cardiol.* 2009;54(24):2277–2286. doi:10.1016/j.jacc.2009.06.055

20. von Bahr L, Batsis I, Moll G, et al. Analysis of tissues following mesenchymal stromal cell therapy in humans indicates limited long-term engraftment and no ectopic tissue formation. *Stem Cells.* 2012;30(7):1575–1578. doi:10.1002/stem.1118

21. Chen G, Park CK, Xie RG, et al. Intrathecal bone marrow stromal cells inhibit neuropathic pain via TGF-beta secretion. *J Clin Invest.* 2015;125(8):3226–3240. doi:10.1172/JCI80883

22. Deer TR, Hayek SM, Pope JE, et al. The polyanalgesic consensus conference (PACC): recommendations for trialing of intrathecal drug delivery infusion therapy. *Neuromodulation.* 2017;20(2):133–154. doi:10.1111/ner.12543

23. Nagel SJ, Reddy CG, Frizon LA, et al. Intrathecal therapeutics: device design, access methods, and complication mitigation. *Neuromodulation.* 2018;21(7):625–640. doi:10.1111/ner.12693

24. Stetkarova I, Yablon SA, Kofler M, et al. Procedure- and device-related complications of intrathecal baclofen administration for management of adult muscle hypertonia: a review. *Neurorehabil Neural Repair.* 2010;24(7):609–619. doi:10.1177/1545968310363585

25. Motta F, Antonello CE. Analysis of complications in 430 consecutive pediatric patients treated with intrathecal baclofen therapy: 14-year experience. *J Neurosurg Pediatr.* 2014;13(3):301–306. doi:10.3171/2013.11.PEDS13253

26. Huang Z, Shen Y, Sun A, et al. Magnetic targeting enhances retrograde cell retention in a rat model of myocardial infarction. *Stem Cell Res Ther.* 2013;4(6):149. doi:10.1186/scrt360

27. Ge R, Li X, Lin M, et al. Fe3O4@polydopamine composite theranostic superparticles employing preassembled Fe3O4 nanoparticles as the core. *ACS Appl Mater Interfaces.* 2016;8(35):22942–22952. doi:10.1021/acsami.6b07997

28. Li J, Wang W, Zhao L, et al. Hydroquinone-assisted synthesis of branched au-ag nanoparticles with polydopamine coating as highly efficient photothermal agents. *ACS Appl Mater Interfaces.* 2015;7 (21):11613–11623. doi:10.1021/acsami.5b02666

29. Fortino VR, Pelaez D, Cheung HS. Concise review: stem cell therapies for neuropathic pain. *Stem Cells Transl Med.* 2013;2 (5):394–399. doi:10.5966/sctm.2012-0122

30. Li X, Wei Z, Li B, et al. In vivo migration of Fe3O4@polydopamine nanoparticle-labeled mesenchymal stem cells to burn injury sites and their therapeutic effects in a rat model. *Biomater Sci.* 2019;7 (7):2861–2872. doi:10.1039/C9BM00242A

31. Bennett GJ, Xie YK. A peripheral mononeuropathy in rat that produces disorders of pain sensation like those seen in man. *Pain.* 1988;33(1):87–107. doi:10.1016/0304-3959(88)90209-6

32. Chaplan SR, Bach FW, Pogrel JW, et al. Quantitative assessment of tactile allodynia in the rat paw. *J Neurosci Methods.* 1994;53 (1):55–63. doi:10.1016/0165-0270(94)90144-9

33. He J, Huang X, Li YC, et al. Self-assembly of amphiphilic plasmonic micelle-like nanoparticles in selective solvents. *J Am Chem Soc.* 2013;135(21):7974–7984. doi:10.1021/ja402015s

34. Xia Y, Tang Z. Monodisperse inorganic supraparticles: formation mechanism, properties and applications. *Chem Commun.* 2012;48 (51):6320. doi:10.1039/c2cc31354e

35. Onakpoya IJ, Heneghan CJ, Aronson JK. Post-marketing withdrawal of 462 medicinal products because of adverse drug reactions: a systematic review of the world literature. *BMC Med.* 2016;14:10. doi:10.1186/s12916-016-0553-2

36. Kola I, Landis J. Can the pharmaceutical industry reduce attrition rates? *Nat Rev Drug Discov.* 2004;3(8):711–715. doi:10.1038/nrd1470

37. Dominici M, Le Blanc K, Mueller I, et al. Minimal criteria for defining multipotent mesenchymal stromal cells. The international society for cellular therapy position statement. *Cytotherapy.* 2006;8 (4):315–317. doi:10.1080/14653240600855905

38. Verdanova M, Rezek B, Broz A, et al. Nanocarbon allotropes-graphene and nanocrystalline diamond-promote cell proliferation. *Small.* 2016;12(18):2499–2509. doi:10.1002/smll.201503749

39. Chen W, Zhang Q, Luk BT, et al. Coating nanofiber scaffolds with beta cell membrane to promote cell proliferation and function. *Nanoscale.* 2016;8(19):10364–10370. doi:10.1039/C6NR00535G

40. Jensen TS, Finnerup NB. Allodynia and hyperalgesia in neuropathic pain: clinical manifestations and mechanisms. *Lancet Neurol.* 2014;13(9):924–935. doi:10.1016/S1474-4422(14)70102-4

41. Maier C, Baron R, Tölle TR, et al. Quantitative sensory testing in the German research network on neuropathic pain (DFNS): somatosensory abnormalities in 1236 patients with different neuropathic pain syndromes. *Pain.* 2010;150(3):439–450. doi:10.1016/j.pain.2010.05.002

42. Park BN, Lim TS, Yoon JK, et al. In vivo tracking of intravenously injected mesenchymal stem cells in an Alzheimer's animal model. *Cell Transplant.* 2018;27(8):1203–1209. doi:10.1177/0963689718788067

43. Sackstein R, Merzaban JS, Cain DW, et al. Ex vivo glycan engineering of CD44 programs human multipotent mesenchymal stromal cell trafficking to bone. *Nat Med.* 2008;14(2):181–187. doi:10.1038/nm1703

44. Liu L, Eckert MA, Riazifar H, et al. From blood to the brain: can systemically transplanted mesenchymal stem cells cross the blood-brain barrier? *Stem Cells Int.* 2013;2013:435093. doi:10.1155/2013/435093

45. Teng Y, Zhang Y, Yue S, et al. Intrathecal injection of bone marrow stromal cells attenuates neuropathic pain via inhibition of P2X4R in spinal cord microglia. *J Neuroinflammation.* 2019;16(1):271. doi:10.1186/s12974-019-1631-0

46. Bradl M, Lassmann H. Oligodendrocytes: biology and pathology. *Acta Neuropathol.* 2010;119(1):37–53. doi:10.1007/s00401-009-0601-5

47. Mu J, Li M, Wang T, et al. Myelin damage in diffuse axonal injury. *Front Neurosci.* 2019;13:217. doi:10.3389/fnins.2019.00217

48. Hunt SP, Pini A, Evan G. Induction of c-fos-like protein in spinal cord neurons following sensory stimulation. *Nature.* 1987;328 (6131):632–634. doi:10.1038/328632a0

49. Coggeshall RE. Fos, nociception and the dorsal horn. *Prog Neurobiol.* 2005;77(5):299–352. doi:10.1016/j.pneurobio.2005.11.002

50. Mert T, Kurt AH, Altun İ, et al. Pulsed magnetic field enhances therapeutic efficiency of mesenchymal stem cells in chronic neuropathic pain model. *Bioelectromagnetics.* 2017;38(4):255–264. doi:10.1002/bem.22038

51. Al-Massri KF, Ahmed LA, El-Abhar HS. Mesenchymal stem cells therapy enhances the efficacy of pregabalin and prevents its motor impairment in paclitaxel-induced neuropathy in rats: role of Notch1 receptor and JAK/STAT signaling pathway. *Behav Brain Res.* 2019;360:303–311. doi:10.1016/j.bbr.2018.12.013

52. Sarveazad A, Janzadeh A, Taheripak G, et al. Co-administration of human adipose-derived stem cells and low-level laser to alleviate neuropathic pain after experimental spinal cord injury. *Stem Cell Res Ther.* 2019;10(1):183. doi:10.1186/s13287-019-1269-y

53. Chen NF, Huang SY, Chen WF, et al. TGF-β1 attenuates spinal neuroinflammation and the excitatory amino acid system in rats with neuropathic pain. *J Pain.* 2013;14(12):1671–1685. doi:10.1016/j.jpain.2013.08.010

54. Cohen SP, Mao J. Neuropathic pain: mechanisms and their clinical implications. *BMJ*. 2014;348:f7656. doi:10.1136/bmj.f7656

55. Mika J, Zychowska M, Popiolek-Barczyk K, et al. Importance of glial activation in neuropathic pain. *Eur J Pharmacol*. 2013;716 (1–3):106–119.

56. Li J, Deng G, Wang H, et al. Interleukin-1beta pre-treated bone marrow stromal cells alleviate neuropathic pain through CCL7-mediated inhibition of microglial activation in the spinal cord. *Sci Rep*. 2017;7:42260. doi:10.1038/srep42260

57. Lin C-H, Wu S-H, Lee -S-S, et al. Autologous adipose-derived stem cells reduce burn-induced neuropathic pain in a rat model. *Int J Mol Sci*. 2017;19(1):34. doi:10.3390/ijms19010034

58. Forouzanfar F, Amin B, Ghorbani A, et al. New approach for the treatment of neuropathic pain: fibroblast growth factor 1 gene-transfected adipose-derived mesenchymal stem cells. *Eur J Pain*. 2018;22(2):295–310. doi:10.1002/ejp.1119